

## THE ROLE OF ACTIVATED DIFFUSION IN THE GASIFICATION OF POROUS CARBONS/CHARS

J.M. Calo and M.T. Perkins  
Chemical Engineering Program  
Division of Engineering  
Brown University  
Providence, Rhode Island 02912

**Keywords:** Activated diffusion; mass transfer resistance; CO<sub>2</sub> gasification.

### INTRODUCTION

The reaction rates of CO<sub>2</sub>, steam, and hydrogen with carbonaceous solids are quite slow, such that the mass transport rate by ordinary bulk diffusion and/or Knudsen diffusion is usually more than sufficient to prevent the reaction from becoming mass transport-limited. Therefore, at first glance the issue of mass transport limitations seems to be relatively unimportant insofar as these reactions are concerned. However, the most reactive carbons are typically those with the highest internal surface areas, and thus it follows that transport in these materials must occur for the most part in pores of molecular dimensions; i.e., micropores. Transport of molecular species into or within micropores does not occur by ordinary bulk diffusion, nor even entirely by Knudsen diffusion. In this case, the energy of interaction between the solid and the gas phase species controls the process. This type of diffusion typically exhibits an Arrhenius-type temperature dependence, and in magnitude is usually slower than Knudsen diffusion. This behavior has been variously known as activated, micropore, intracrystalline, configurational, and surface diffusion [1]. Even though these terms are often used interchangeably in the literature, they may also refer to completely different mechanisms in different systems.

In the current paper we present some measurements of effective diffusion times in coal chars obtained using a transient technique, and analyze the results in terms of their potential effect on CO<sub>2</sub> gasification reactivity.

### EXPERIMENTAL

The apparatus for measuring the effective diffusion times consists of: (1) a continuous gas flow, fixed solids, "gradientless" reactor, for carrying out the reaction under well-mixed conditions; (2) a solenoid/control valve network for generating step function changes in feed composition under conditions of constant flow rate, temperature, and pressure; (3) a supersonic molecular beam mass spectrometer system for measuring the transient response of the gas phase composition in the reactor effluent; and (4) a microcomputer for automated data logging and mass programming of the mass spectrometer [2]. In the current work, the highest operating temperature was 1273K and the highest pressure was 90 psig, although most of the data were obtained at a pressure of 30 psig. The reactor space time could be varied from about 0.01 to 2.0 min.

#### *Sample Preparation.*

Buller coal (New Zealand, medium volatile bituminous) activated char samples were supplied by Sutcliffe-Speakman Carbons Ltd. of Lancashire, England. The three other coals used in this study (PSOC-467 [Deadman #2] subbituminous, PSOC-833 [Fort Union Bed] lignite, and Wyodak subbituminous) were pyrolyzed in a tube furnace in ~50g batches at 1000°C under UHP nitrogen. Chars from the same coal produced in different batches were mixed. This large sample was divided up into reactor sample aliquots of 60-80g, and smaller characterization samples. The chars were sieved to a mean particle size of 1.6 mm. This size was selected primarily because it ensures complete retention

of the sample in the basket during operation, and yet provides minimal pressure drop through the sample bed. In addition, a mean particle size of 0.8 mm yielded results similar to those for 1.6 mm particles; i.e.,  $\pm 5\%$  for  $\text{CO}_2$  diffusion in PSOC-467; therefore, additional particle size tests were not conducted. Once loaded in the sample basket, the chars were heated to  $150^\circ\text{C}$  for one hour to remove adsorbed water vapor.

#### *Experimental Procedures.*

A typical experiment was conducted as follows. The sample ( $60\text{--}80\text{ cm}^3$ ) was placed in the sample basket, and positioned in the Berty reactor. A sheath-type thermocouple was inserted into the sample bed, and another was located in the free gas volume of the reactor. The reactor was then sealed and purged with argon. The reactor furnace was then turned on. After attaining operating temperature, the solenoid valve gas addition circuit was used to introduce the gas of interest as a step function change in concentration. The flow rates of the different gases were balanced such that the pressure in the reactor remained constant during the transient experiment. The reactor effluent concentration was then continuously monitored with the mass spectrometer, and the data were logged automatically. Runs typically required less than four minutes, following which the reactor was quickly refilled with argon using the gas addition flow circuit.

#### DATA ANALYSIS PROCEDURE

The experiment generates a time-concentration trace of the reactor effluent. A variety of analysis techniques were investigated to extract diffusion information from these data. A "difference" technique was finally selected. It is based on the "difference" variable,  $\Delta C = C - C^*$ , where  $C$  and  $C^*$  are the time-dependent concentrations in a well-mixed reactor both without and with a porous material sink present. The corresponding differential mass balance is given by:

$$\frac{\partial \Delta C}{\partial t} = -\frac{\Delta C}{\tau} + 3\frac{D_e}{R^2} \frac{\partial C^\dagger}{\partial r} \left( \frac{V_s}{V_g} \right) (1 - \epsilon_b)(1 - \epsilon_m), \quad [1]$$

where  $t$  is time,  $\tau$  is the reactor space time at reactor conditions,  $R^2/D_e$  is the effective diffusion time within the char,  $V_{s,g}$  are the solids bed and free gas volumes within the reactor, respectively,  $\epsilon_{b,m}$  are the external bed and intraparticle macropore void volumes, respectively, and  $\partial C^\dagger/\partial r$  is the dimensionless concentration gradient at the surface of the microporous regions (assumed to be spherical). When  $\Delta C$  is a maximum,  $\partial \Delta C/\partial t = 0$ , and Eq. [1] becomes:

$$\frac{\Delta C^{\max}}{\tau} = 3\frac{D_e}{R^2} \frac{\partial C^\dagger}{\partial r} \left( \frac{V_s}{V_g} \right) (1 - \epsilon_b)(1 - \epsilon_m) \text{ at } t=t^{\max} \quad [2]$$

This expression requires the specification of  $\partial C^\dagger/\partial r$  at the external surface of the "microparticle." This was estimated by the analytical expression for the gradient at the surface of a spherical particle driven by a "gradientless" reactor with the same space time [3]; viz.,

$$\frac{\partial C^{\dagger}}{\partial r} \Big|_{r=R} = e^{-t/\tau} \left( 1 - \frac{R^2}{\tau D_e} \cot \left\{ \frac{R^2}{\tau D_e} \right\}^{\frac{1}{2}} \right) - 2 \left( \frac{R^2}{\tau D_e} \right) \sum_{n=1}^{\infty} (-1)^n \frac{e^{-D_e n^2 \pi^2 / R^2}}{\left( n^2 \pi^2 - \frac{R^2}{\tau D_e} \right)} \quad [3]$$

An iterative approach is required to solve the resultant Eq. [2] for  $R^2/D_e$ . Subsequently, the forcing function was generated from the data itself for an improved approximation.

In Figure 1 are presented some representative data for CO diffusing into PSOC-833 coal char at 285°C and 30 psig. The response of a hypothetical run at the same reactor space time with no porous char mass sink (i.e., C) is also presented, as well as the difference curve,  $\Delta C$ . The maximum is located at  $C/C_0 = 0.25$  and  $t = 33$  s. Next, the data were fit to the expression  $[1 - \exp(-t/\tau_{eff})]$  to find  $\tau_{eff}$ . For the data in Figure 1, the best fit is for  $\tau_{eff} = 42.1$  s ( $\tau = 25.9$  s). The resultant simple rising exponential expression is then used as the external forcing function to find the concentration gradient at the microparticle external surface. The best fit value of  $R^2/D_e$  is then found *via* an iterative search. For the data presented in Figure 1, the best fit value was  $D_e/R^2 = 0.0134$  s<sup>-1</sup>.

## RESULTS AND DISCUSSION

### *Characteristic Diffusion Time Results.*

All the results exhibited an increase in effective diffusivity with temperature. However, in general, the Arrhenius plots of the results were not very linear. Much of the data indicated a concave downward curvature which could be indicative of a change in mechanism of the transport mechanism with temperature. "Best fit" Arrhenius parameters over the entire temperature range are presented in Table I. As shown, the measured activation energies range from about 0.1 to 1.8 kcal/mole. The apparent activation energy of CO<sub>2</sub> was typically the largest of the gases studied in each coal char.

For a Wyodak coal char, Debelak [4] reported values for CH<sub>4</sub> varying from 0.9 - 3.2 kcal/mol, and values for CO<sub>2</sub>, CO, and N<sub>2</sub> from 0.5-2.6 kcal/mol, over a temperature range of 50 to 250°C. A comparison of the current results for CO<sub>2</sub> diffusion in pre-oxidized (with air) Wyodak with the corresponding results of Debelak [4] is presented in Figure 2. Since high temperature surface cleaning, nor oxygen chemisorption in air were performed in the latter work, the actual state of the surface is uncertain. However, both sets of data still agree reasonably well. The observed differences are attributed to the different modes of burn-off (i.e., in CO<sub>2</sub> vs. O<sub>2</sub>), which may have resulted in different porosity morphologies.

The magnitudes of the apparent activation energies from the current data are relatively low, which in some cases might be due to the influence of Knudsen diffusion. Arrhenius plots of Knudsen diffusivities ( $D_K \propto T^{1/2}$ ) exhibit a noticeable upward curvature, with the slope increasing with temperature. The PSOC-467 coal char had the largest mean pore radius of the coal chars examined. However, the Arrhenius plots for CO and CO<sub>2</sub> diffusion in PSOC-467 did not exhibit an increasing negative slope with temperature, characteristic of Knudsen diffusion. Thus, it is concluded that Knudsen diffusion was not dominant over the entire temperature range examined.

### *The Effect of Pressure.*

Figure 3 demonstrates the effect of CO<sub>2</sub> pressure on the apparent diffusivity of CO<sub>2</sub> in PSOC-833 coal char at 285°C. As shown, there is a marked *decrease* in apparent diffusivity with increasing pressure for CO<sub>2</sub> pressure. In terms of classical models for activated diffusion, this is consistent with an

*occluded gas model* where diffusion occurs on the surface by jumping from one adsorption site to another [5]. Increasing pressure tends to populate the adsorption sites, thereby decreasing the diffusion rate.

#### **The Effect of Burn-Off.**

Samples of the Wyodak coal char were burned-off in an air fluidized bed at 300°C for intervals of about 2 hours. In between runs, the samples were weighed, and the burn-off determined. The effective surface areas for the Wyodak coal char increased with burn-off, attaining 518 m<sup>2</sup>/g (by CO<sub>2</sub> BET; 450 m<sup>2</sup>/g by N<sub>2</sub> BET) for the 30% burn-off sample.

As shown in Table I, E<sub>D</sub> for the three gases generally seem to increase with burn-off, although this is not a universal trend. At the lower burn-offs in oxygen, the Wyodak coal char develops microporosity with burn-off, but the pore size distribution does not change radically [2]. However, simultaneously the remaining mineral matter is continually being concentrated at pore walls. This effect is known to enhance specific reactivity in chars with catalytic mineral matter impurities [6]. If a diffusing gas interacts strongly with the mineral matter, then this could explain the general activation energy increase with burn-off. This hypothesis is not supported by the slightly higher apparent activation energies observed for CO<sub>2</sub> and CH<sub>4</sub> in the "0% burn-off" demineralized Wyodak coal char. However, the demineralization procedure [7] is known to significantly affect the porosity, and thus a better comparison might be with a higher burn-off sample. Thus, it is noted that all three E<sub>D</sub> values are higher for the 10.1% burn-off sample than the demineralized sample, although this result is not conclusive.

The sharp decrease in E<sub>D</sub> for CO evident at 30% burn-off may be due to the measured shift of the pore size distribution towards larger pore radii for this char sample [2]. CO, being the smallest of the three molecules may be the most sensitive to the microporosity morphology.

#### **Mass Transfer Limitations.**

In order to explore the potential effect of mass transfer resistance on reactivity, a classical "effectiveness factor" ( $\eta$ ) analysis was performed. CO<sub>2</sub> gasification reactivities were measured for the four coal chars investigated in a thermogravimetric apparatus (TGA) under 0.1 MPa of CO<sub>2</sub>. A simple first order rate expression was assumed for the rate form. Initially, assuming no mass transport resistance (i.e.,  $\eta = 1$ ), the Thiele modulus,  $\phi = \{[k_1/(D_c/R^2)]^{1/2}\}/3$  ( $k_1$  is the first order rate constant), can be calculated from the measured reaction rate and the effective diffusion time. (For temperatures higher than those for which data were obtained,  $D_c/R^2$  values were extrapolated using the measured apparent activation energy.) Knowing  $\phi$ ,  $\eta$  can be determined from the well-known analytical expression,  $\eta = 1/[(1/\tanh(3\phi)) - 1/(3\phi)]$ . This value can then be used to correct  $\phi$ , and the process is iterated until  $\eta$  and  $\phi$  agree.

The resultant effectiveness factors determined for the coal chars investigated, over a temperature range of 1073-1173K, are presented in Figure 4. As shown,  $\eta < 1$  for all the coal chars, and  $\eta \ll 1$  at 1173K, indicating almost complete mass transport control under the latter conditions. The most severely transport-limited char is the Buller (activated) coal char, while the least affected are the PSOC-833 and PSOC-467 coal chars. This is consistent with the fact that the activated Buller coal char was the most microporous, while the PSOC samples were the least microporous, since they experienced little burn-off. As might be expected, the Wyodak samples at progressive burn-offs were intermediate between these two extremes.

## CONCLUSIONS

Activated transport through microporous coal chars does not appear to be generally describable by a single simple model. The behavior depends on the diffusing species and char porosity morphology and composition, as well as surface site occupancy [2]. For the results that exhibited a pressure effect, the occluded phase model appears to be more applicable. However, some of the results exhibited a decrease in apparent activation energy at high temperatures that is characteristic of two-phase model behavior. Most of the results exhibit behavior somewhere in between these two extremes. Thus, the actual mechanism is likely to be a combination of these two processes, and, possibly, others (e.g., Knudsen diffusion) as well.

The reaction of CO<sub>2</sub> with coal char should be mass transport-controlled in the microporosity for all the coal chars examined at temperatures greater than about 800°C, with  $\eta < 0.2$  for all the samples under these conditions. In addition, the CO<sub>2</sub> reactivity of Wyodak coal char would still appear to be mass transport-limited up to 30% burn-off.

**Acknowledgements.** This work was supported by the Department of Energy under Grant No. DE-FG22-86PC90529 from the Pittsburgh Energy Technology Center. The authors also wish to thank Sutcliffe-Speakman Carbons Ltd. of Lancashire, England for providing activated carbon samples.

## REFERENCES

1. Ruthven, D.M., *Principles of Adsorption and Adsorption Processes*, Wiley, NY, 1984.
2. Calo, J.M., and M.T. Perkins, *Micropore Diffusion in Coal Chars Under Reactive Conditions*, DOE Final Tech. Report, DE-FG22-86PC90529F, May, 1990.
3. Crank, J., *The Mathematics of Diffusion*, 2nd ed., Oxford Univ. Press, 1975.
4. Debelak, K., *Influence of Changing Particle Structure on the Rate of Gas-Solid Gasification Reactions*, DOE Final Tech. Report, DE-AC21-81MC16053-F, August, 1983.
5. Palekhar, M.G., and Rajadhyaksha, R.A., *J. Cat. Rev.-Sci. Eng.* **28**, 382 (1986).
6. Solomon, P.R. and J.M. Beér in *Coal Gasification: Direct Applications and Syntheses of Chemicals and Fuels*, DOE Coal Gasification Research Needs Working Group, June 1987.
7. Morgan, M.E., Jenkins, R.G., and Walker, P.L., Jr. *Fuel* **60**, 189 (1981).

Table I. Summary of parameters for  $D_e/R^2 = (D_e/R^2)_0 \exp(-E_D/RT)$ .

<u>Char</u>	<u>Species</u>	$(D_e/R^2)_0$ (s <sup>-1</sup> )	$E_D$ (kcal/mol)
Buller "B" (steam activated)	CO	0.022	0.32
	CO <sub>2</sub>	0.029	1.2
	CH <sub>4</sub>	0.047	1.4
PSOC-833 {17.1% burn-off in 0.1MPa O <sub>2</sub> at 200°C (pre-oxidized)}	CO	0.012	0.57
	CO <sub>2</sub>	0.16	1.8
	CH <sub>4</sub>	0.028	0.42
PSOC-467 {13.2% burn-off in 0.1MPa O <sub>2</sub> at 200°C (pre-oxidized)}	CO	0.09	0.82
	CO <sub>2</sub>	0.042	0.86
Wyodak {0% burn-off; as pyrolyzed ("clean")}	CO	0.012	0.32
	CO <sub>2</sub>	0.033	0.87
	CH <sub>4</sub>	0.041	0.75
Wyodak {10.1% burn-off in 0.1MPa O <sub>2</sub> at 200°C (pre-oxidized)}	CO	0.041	1.1
	CO <sub>2</sub>	0.056	1.4
	CH <sub>4</sub>	0.41	1.3
Wyodak {15% burn-off in 0.1MPa O <sub>2</sub> at 200°C (pre-oxidized)}	CO	0.084	1.7
	CO <sub>2</sub>	0.045	1.3
	CH <sub>4</sub>	0.031	0.37
Wyodak {30% burn-off in 0.1MPa O <sub>2</sub> at 200°C (pre-oxidized)}	CO	0.024	0.42
	CO <sub>2</sub>	0.15	1.8
	CH <sub>4</sub>	0.095	1.1
Wyodak {0% burn-off; demineralized}	CO	0.028	0.11
	CO <sub>2</sub>	0.072	1.1
	CH <sub>4</sub>	0.088	0.92

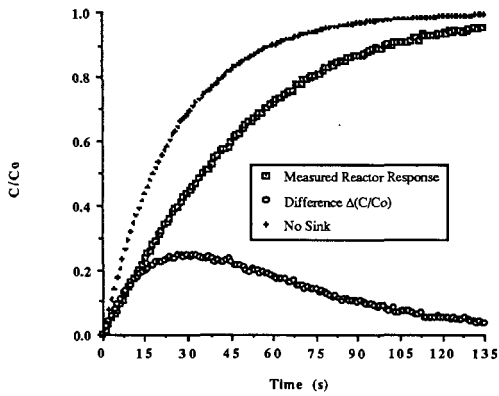


Figure 1. Data for CO diffusing into PSOC-833 coal char at  $T=285^{\circ}\text{C}$  and  $P=30$  psig, and theoretical response of a reactor with no internal porous mass sink under the same conditions.

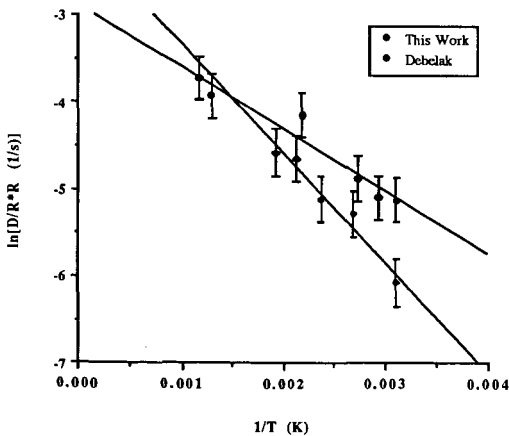


Figure 2. Comparison of activated diffusivities for  $\text{CO}_2$  in Wyodak coal char in this work (10.1% burn-off in air) to those obtained by Debelak [4] (17.6% burn-off in  $\text{CO}_2$ ).

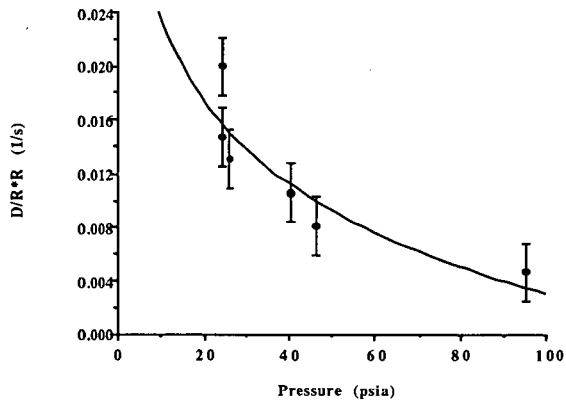


Figure 3. Effect of CO<sub>2</sub> pressure on effective diffusion time in PSOC-833 at 285°C.

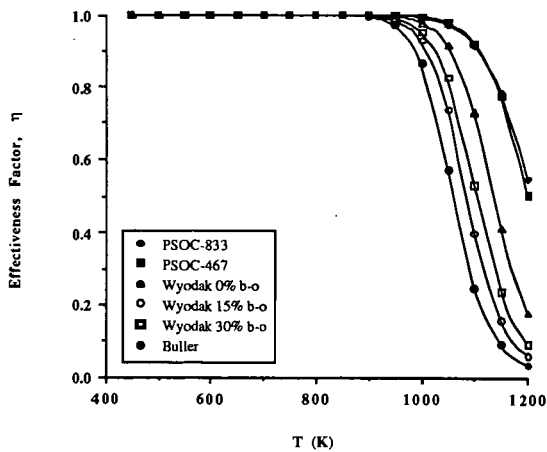


Figure 4. Calculated effectiveness factors for all the coal chars investigated.